Phase-Coupled Plasmon-Induced Transparency

Rohan D. Kekatpure, Edward S. Barnard, Wenshan Cai, and Mark L. Brongersma*

Geballe Laboratory for Advanced Materials, Stanford University, Stanford, California 94305, USA

(Received 10 February 2010; revised manuscript received 22 March 2010; published 17 June 2010)

We demonstrate the existence of electromagnetically-induced-transparency (EIT-)like spectral response in a system of nanoscale plasmonic resonator antennas coupled by means of a single-mode silicon waveguide. Our proposed scheme exploits the *phase* of the coupling between the antennas in contrast with the existing plasmonic approaches that rely on the *strength* of direct, near-field coupling of nanometallic elements. Quality factors of over 100 and group indices of over 10 are readily achieved at near-infrared frequencies by a single unit in $\approx 1\ \mu m^2$ of total device footprint, representing a more than two orders size reduction over corresponding dielectric EIT structures. By obviating the need for a near-field interaction, the phase-coupling scheme also facilitates an improved access to the coupling medium between the resonators thereby paving the way toward dynamic control of their sharp EIT-like spectral response.

DOI: 10.1103/PhysRevLett.104.243902 PACS numbers: 42.82.Et, 42.50.Gy, 78.67.Pt

Electromagnetically induced transparency (EIT) is a laser-activated enhancement of transmission in a material's absorption band resulting from a coherent interaction between the atomic levels and the applied optical fields [1]. By enabling low-loss transmission through the absorption band, EIT allows the use of the strong dispersion usually accompanying an absorption resonance. The strong dispersion is the key to achieving a dramatic group-velocity-reduction in propagating light pulses and to realizing diverse phenomena including enhanced optical nonlinearities, ultrafast switching, and optical data storage [2]. Requirements of macroscopic apparatus, stable gas lasers, and low temperature environments make the conventional realization of EIT unsuitable for chip-scale implementation, where a majority of the proposed applications are envisioned. This realization has catalyzed an ongoing search for classical systems mimicking EIT. Various resonant dielectric systems including coupled microdisks, photonic crystals, and microrings have been proposed and demonstrated to display EIT-like spectral response [3–5].

Plasmonic structures such as fish scales [6], split-ring resonators [7], and dipole-qudrupole couples [8,9] are the most recent and promising additions to the existing array of classical EIT schemes. Metallic structures are especially appealing as they offer a strong optical response from a subwavelength object, enabling exploration of the ultimate scaling limits of this phenomenon.

The EIT-like spectral response exhibited by classical structures are understood to arise from normal-mode splitting of a low-Q (radiative) resonator induced by its coupling with a high-Q (dark) resonator [8] or from destructive interference between parallel excitation pathways of a radiative antenna [9]. Viewed either way, a near-field coupling of the two nanoantennas or resonators is essential in these schemes for the observation of the EIT-like spectra. These near-field coupling schemes hinge on the *strength* of the coupling between constituent nanoantennas and entail interantenna separations on the order of tens of nanometers [6–10]. Such spacings, in addition to requiring a precise lithographic control, restrict the access to the coupling medium between the antennas.

In this Letter, we show how the *phase* of the coupling between the nanoantennas may be exploited to obviate the requirement of near-field coupling. In lieu of the near fields, a well-defined phase coupling can be established between resonators via a single-mode waveguide—a concept already familiar in dielectric waveguide optics [5]. We will show that translation of this concept into the plasmonic realm promises to shrink the structure footprint by over two orders, while simultaneously bringing about considerable design simplifications.

The most noteworthy advantages of the phase-coupling scheme are its feasibility in a planar waveguide configuration and an unimpeded access to the interantenna coupling medium. Weak response of individual EIT units typically calls for light to interact in succession with an array of these units. For near-field-coupled EIT structures, three-dimensional stacks have been proposed as a means to increase the interaction length [6,8,9]. In the phase-coupling scheme, such an array of EIT units may conveniently be laid alongside a single-mode waveguide permitting practically arbitrary interaction lengths. An access to the coupling medium exposed between two phase-coupled antennas can facilitate new types of passive sensing structures and a dynamic control of their EIT-like response. Such a control could enable new fundamental studies of EIT dynamics and help realize the next generation of ultracompact, THz-speed electro-optic devices including, modulators, switches, and tunable delay lines.

We introduce the phase-coupled plasmon-induced transparency (PC-PIT) scheme by referring to the schematic in Fig. 1(a) showing two antennas with a separation s on top of a single-mode Si waveguide. Recent work has demonstrated that metallic stripes depicted in Fig. 1(b) can serve as plasmonic antennas, which behave as resonators for surface plasmon polaritons and allow effective coupling to the

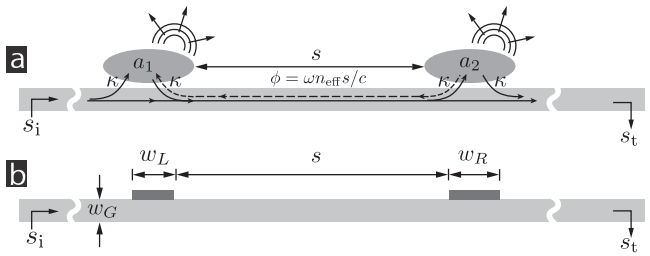

FIG. 1. (a) The lumped structure used for analytical modeling of the phase-coupled plasmon-induced transparency (PC-PIT) structure. (b) A plasmonic realization of the PC-PIT scheme using coupled metal-stripe antennas.

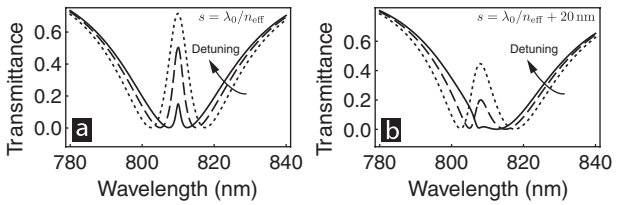

FIG. 2. Spectral transmittance of a generic coupled resonator system calculated using analytical coupled-mode theory. The parameters are $\lambda_0 = 810$ nm, $\gamma_1 = \gamma_2 = 3 \times 10^{13}$ s^{-1}, and $\kappa = \sqrt{\gamma_1}$. (a) Spectral transmittance for the case in which the interantenna spacing is matched to the resonant wavelength λ_0: $s = \lambda_0/n_{\text{eff}}$ for antenna detuning of 5 nm (solid), 10 nm (dashed), and 15 nm (dotted). (b) Spectral transmittance for the same set of antenna detunings but with the interantenna spacing mismatched by 20 nm: $s = \lambda_0/n_{\text{eff}} + 20$ nm.

outside world [11,12]. In the configuration of Fig. 1(b), the antennas primarily interact with the much higher index Si waveguide and can be treated as side-coupled cavities. Using coupled-mode theory [13], the time-harmonic energy amplitudes a_1 and a_2 of the antennas in Fig. 1(b) can be expressed according to

$$\begin{bmatrix} a_1 \\ a_2 \end{bmatrix} = \begin{bmatrix} \delta\omega_1 - i\gamma_1 & i|\kappa|^2 e^{-i\phi} \\ i|\kappa|^2 e^{-i\phi} & \delta\omega_2 - i\gamma_2 \end{bmatrix}^{-1} \begin{bmatrix} \kappa s_i \\ -\kappa s_i e^{-i\phi} \end{bmatrix}. \tag{1}$$

Here $\delta\omega_{1,2} = \omega - \omega_{1,2}$ are the deviations of the natural (uncoupled) antenna resonance frequencies $\omega_{1,2}$ from the input frequency ω, κ is the fraction of power coupling into the waveguide, and $2\gamma_{1,2}$ is the energy-decay rate out of the uncoupled antennas. The difference $|\omega_1 - \omega_2|$ of the uncoupled antenna resonance frequencies is termed *detuning* and is a design parameter that can be tailored to obtain a desired spectral response. For a waveguide mode with an effective index n_{eff}, the phase accumulated in propagating between the resonators is $\phi = \omega n_{\text{eff}} s/c$.

Equation (1) exhibits a number of similarities to the one used to model the near-field-coupled EIT structures [8]: the diagonal terms arise from the individual antennas and the off-diagonal terms represent the coupling. The crucial difference distinguishing the present case is the appearance of the phase term $e^{-i\phi}$ accompanying the coupling strength κ. The right-hand side of the equation also highlights the relative phase acquired by the input field between its coupling to the two antennas. We may write the transmitted power amplitude as

$$s_t = -e^{i\phi}(-s_i - i\kappa a_1) - i\kappa a_2. \tag{2}$$

Eqs. (1) and (2) yield the transmittance $|s_t/s_i|^2$ after elimination of the energy amplitudes a_1 and a_2.

Figure 2 illustrates how the EIT-like spectral response of PC-PIT structures can be altered in two ways. First, it can be tailored by modifying the resonance frequencies individual antennas through a choice of their geometrical parameters (e.g., stripe width). Second, the peak transmittance of the coupled-antenna system can be modified by changing the antenna spacing. Figure 2 shows the analytically calculated transmittance ($|s_t/s_i|^2$) of the coupled antennas for three different detunings of the individual antenna resonance frequencies from the coupled-antenna resonance. Figure 2(a) shows the case for which the coupled-antenna system is on resonance at 810 nm. Figure 2(b) shows the situation for the same antennas, but now with the antennas separated by an additional 20 nm. These figures illustrate several important rules for design of PC-PIT structures. Most notably, the antenna detuning provides a direct means to control the Q of the EIT-like resonance. If coupling to waveguide were the only decay pathway for the antenna energy, the detuning would allow for realization of arbitrarily narrow spectral widths while retaining unity peak transmission. With other decay channels present, however, smaller antenna detuning leads to a drop in peak transmittance as seen in Fig. 2(a), thus offering a trade-off between Q and peak transmission. It is also important to note that a strong EIT-like peak is observed only for certain values of the antenna separation s. The EIT resonance is weak or quenched if s lies outside the range of those values. Interestingly, sharper EIT peaks are more sensitive to the value of s. For example, the sharp EIT peak in Fig. 2(a) for a 5 nm antenna detuning is significantly quenched in Fig. 2(b) for a 20 nm variation in s. While an off-resonant value of s does reduce the peak transmission in the case of 15 nm antenna detuning, the response is still distinctly observable in Fig. 2(b).

Armed with these design guidelines, we now for the first time propose a plasmonic realization of the PC-PIT scheme and illustrate its operation through rigorous numerical calculations. Our proposed structure, shown in Fig. 1(b), consists of two antennas on top of a 100 nm thick silicon waveguide. For the present PC-PIT structure, we choose 30 nm thick silver antennas having widths w_L and w_R and an inner-edge separation s. The complex permittivity of silicon is taken to be $\epsilon_{\text{Si}} = 12.25 - i0.021$ and that of silver is determined using the Drude model: $\epsilon_{\text{Ag}} = \epsilon_\infty - \omega_p^2/(\omega^2 - i\omega\Gamma)$ with $\epsilon_\infty = 4.38$, $\omega_p = 1.37 \times 10^{16}$ s^{-1}, and $\Gamma = 3.07 \times 10^{13}$ s^{-1} [8]. The numerical calculations are carried out using the commercial finite element method package COMSOL Multiphysics.

Normalized transmittances of the individual and coupled antennas were obtained by dividing their transmission spectra with that of an isolated 100 nm thick silicon waveguide (which is very high given the decay length of about 40 μm for the waveguide mode at 810 nm).

Figure 3, (A1–C1) show the power transmittance spectra of the individual antennas comprising the coupled system. The left antenna width is $w_L = 290$ nm leading to a resonance dip at 795 nm. The width of this antenna is held fixed as the right antenna width is varied between 300–320 nm. As expected, the two resonance dips approach each other with decreasing difference of the antenna widths. The remaining subfigures in Fig. 3 show the transmittance of the coupled antennas as the spacing between them is varied from 600 to 800 nm in steps of 40 nm. All three antenna systems show the transparency band between the individual antenna resonances. For a given inner-edge spacing, the full-width at half-maximum (FWHM) and the peak transmittance ($T_{\max}$) of the transparency window increase dramatically with an increasing antenna detuning. For a given antenna detuning, $T_{\max}$ and FWHM vary nonmonotonically with s, reaching a maximum around $s = 720$ nm in all three cases. Furthermore, the shape of the transparency window is less sensitive to s for larger detuning. Each of these numerical results is consistent with the analytical model presented in Fig. 2.

The spacing dependence of the transparency spectra in Fig. 3 inspires yet another physical picture of the phase-coupled structures as a Fabry-Pérot (FP) resonator with frequency-dependent end-mirror reflectivities. Spectral transmission of a two-mirror FP resonator can be expressed as

$$T_{\mathrm{FP}}(\omega) = \left| \frac{t_1(\omega)t_2(\omega)}{1 - r_1(\omega)r_2(\omega)e^{i2\beta(\omega)s}} \right|^2, \qquad (3)$$

where $r_{1,2}(\omega)$ ($t_{1,2}(\omega)$) are frequency-dependent reflection (transmission) coefficients of the two point mirrors with a separation s, and $\beta = \omega n_{\mathrm{eff}}/c$ is the propagation constant of the waveguide mode coupling the mirrors. The transmittance of the mirrors are obtained from Fig. 3 (A1–C1) and are related to the reflectance according to $|r_{1,2}(\omega)|^2 = \eta - |t_{1,2}(\omega)|^2$. $\eta = 1$ if mirror transmittance is the only source of power loss. For metal-stripe antennas, scattering into free-space modes and resistive losses make $\eta < 1$. Transmittance of the coupled-antenna system calculated using the FP model ($\eta = 0.3$) is plotted using solid lines in Fig. 3. Despite its simplicity, the FP model superbly predicts the spectral transmittance of the PC-PIT system using just the individual antenna response. The slight mismatch with numerical results is caused by the finite mirror size in real structures, which introduces uncertainty in the value of s. The operation of the PC-PIT system and its correspondence with the FP model is visually illustrated in Fig. 4 that shows the amplitude of the magnetic field at the three wavelengths indicated in Fig. 3, A5. From Figs. 4(a) and 4(c), the transmission dips at $L1$ and $L2$ in Fig. 3, A5 to correspond to the resonances of the individual antennas. At these wavelengths, only a minimal power exists in the silicon waveguide past the two antennas. In the FP model, these points correspond with the strong reflectivity of the individual mirrors. At the transparency peak M, *both* antennas are partially resonant with individual reflectivities less than their maximum as seen in

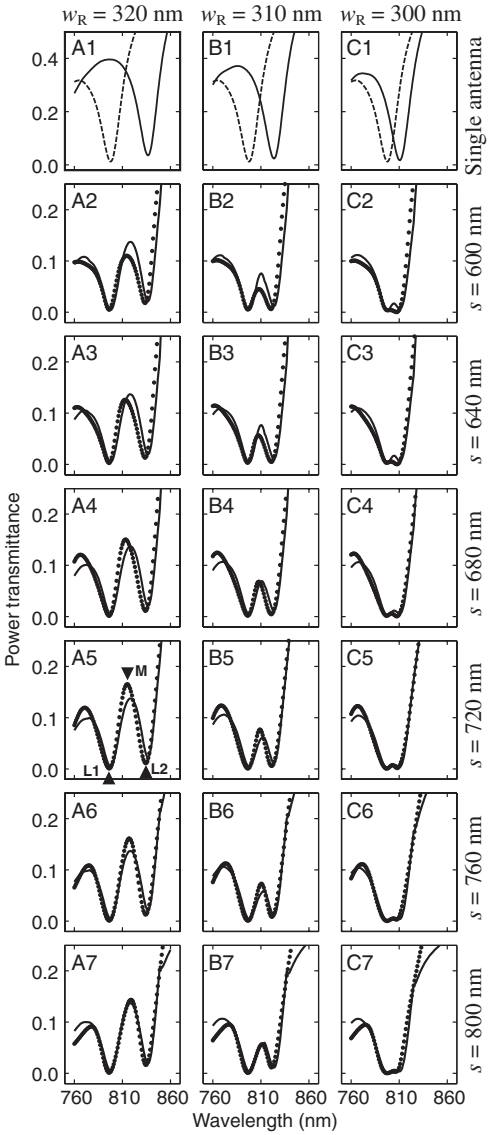

FIG. 3. Power transmission of isolated and coupled Ag stripe antennas. A1, B1, and C1 show the resonances of the individual antennas. The dashed lines in all three subfigures is the transmittance of a single 290 nm stripe. The solid curves are the transmission spectra of 320 nm (A1), 310 nm (A2), and 300 nm (A3) wide stripes and show the detuning with the 290 nm stripe. Subfigures 2–7 are the transmittances of the coupled stripes with $w_L = 290$ nm and $w_R = 320$ nm (A2–A7), $w_R = 310$ nm (B2–B7), $w_R = 300$ nm (C2–C7) for the inner edge the separations as indicated on the far right. The dotted lines indicate the simulation wavelengths and the solid lines are the analytical fits using the Fabry-Pérot model Eq. (3). Black triangles in A5 indicate the wavelengths used for field plots in Fig. 4.

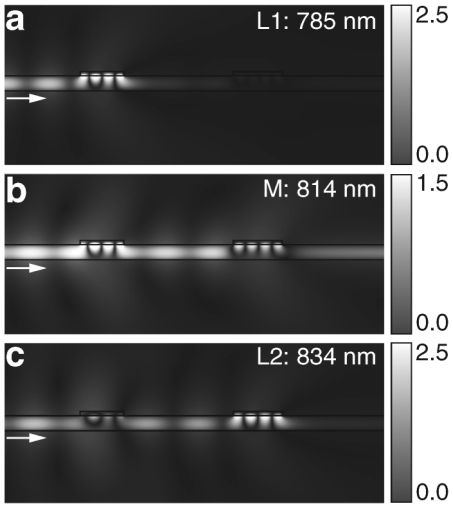

FIG. 4. Normalized magnetic field $|\mathbf{H}/\mathbf{H}_0|$ at the three wavelengths indicated by $L1$, $L2$, and M in Fig. 3, A5. (a) and (c) correspond to the individual resonances ($L1$ and $L2$) of the stripes while (b) is the EIT-like resonance M of the coupling region. $\mathbf{H}_0$ is the magnetic field of an isolated waveguide at the indicated wavelengths. The incidence direction is indicated by the white arrow.

Fig. 4(b). The waveguide region between the antennas acts as a FP cavity bounded by two partially reflecting antennas. Further, if the antenna spacing at this wavelength equals integer half-wavelengths, this cavity is resonant and displays a transmission maximum. A significant amount of power is seen exiting the waveguide past the antennas. The FP cavity-model thus qualitatively and quantitatively explains the spectra in Fig. 3 and is a powerful tool for design of PC-PIT systems.

Next, we quantify the refractive index dispersion and the group-index achieved in the PC-PIT scheme. The frequency dependence of the refractive index is determined by transforming the spectral transmittance to an effective absorption coefficient $\alpha(\omega) = -\ln T(\omega)/s$ and subsequently using the Kramers-Kronig relations to transform the $\alpha(\omega)$ to refractive index. The group-index n_g is obtained from $n(\omega)$ as $n_g(\omega) = n(\omega) + \omega dn(\omega)/d\omega$. The effective material index evaluated using this procedure is plotted in Fig. 5. Group indices of up to 14 are achieved by a single coupled-antenna unit. The antenna detuning allows for a direct trade-off between the peak value of n_g and bandwidth over which it is observed highlighting the well-known bandwidth-delay limit for EIT-like systems [7]. For an antenna spacing of 720 nm, the bandwidth-delay product for our system is constant at $13 \pm 2\%$ and is comparable to that obtained using split-ring resonators [7]. As seen in Fig. 3, antenna detuning also dictates the peak transmittance, indicating that high n_g values come at the expense of increased absorption.

In summary, we have numerically demonstrated EIT-like high-Q spectral response in waveguide-coupled metal-stripe antennas. Phase coupling obviates the need for a near-field interaction and opens up a pathway toward dynamic control of the spectral response. Antenna detuning is the key parameter controlling the peak-transmittance, Q, and the maximum pulse delay. Group indices of >10 and $Q > 100$ can be achieved within a device footprint of ≈ 1 μm^2. This small footprint together with the tunable, and narrow linewidth spectral response can actualize a new class of hybrid dielectric-plasmonic structures and active devices for fundamental study and applications.

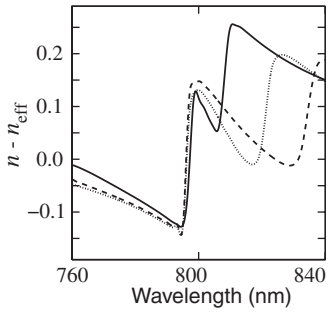

FIG. 5. Spectral variation of the effective material index calculated from EIT transmission spectra using the Kramers-Kronig relations. The three curves represent various degrees of antenna detuning and are calculated from Fig. 3 (A5–C5) corresponding to $w_R = 320$ nm (solid line), 310 nm (dashed line), and 300 nm (dotted line).

The authors acknowledge the support of the Interconnect Focus Center, one of six research centers funded under the Focus Center Research Program (FCRP), a Semiconductor Research Corporation entity.

*brongersma@stanford.edu

[1] K.-J. Boller, A. Imamoglu, and S. E. Harris, Phys. Rev. Lett. **66**, 2593 (1991).
[2] T. F. Krauss, Nat. Photon. **2**, 448 (2008).
[3] L. Maleki, A. B. Matsko, A. A. Savchenkov, and V. S. Ilchenko, Opt. Lett. **29**, 626 (2004).
[4] M. F. Yanik, W. Suh, Z. Wang, and S. Fan, Phys. Rev. Lett. **93**, 233903 (2004).
[5] Q. Xu *et al.*, Phys. Rev. Lett. **96**, 123901 (2006).
[6] N. Papasimakis, V. A. Fedotov, N. I. Zheludev, and S. L. Prosvirnin, Phys. Rev. Lett. **101**, 253903 (2008).
[7] P. Tassin, L. Zhang, T. Koschny, E. N. Economou, and C. M. Soukoulis, Phys. Rev. Lett. **102**, 053901 (2009).
[8] S. Zhang, D. A. Genov, Y. Wang, M. Liu, and X. Zhang, Phys. Rev. Lett. **101**, 047401 (2008).
[9] N. Liu *et al.*, Nature Mater. **8**, 758 (2009).
[10] F. Hao *et al.*, Nano Lett. **8**, 3983 (2008).
[11] E. S. Barnard, J. S. White, A. Chandran, and M. L. Brongersma, Opt. Express **16**, 16 529 (2008).
[12] S. I. Bozhevolnyi and T. Sondergaard, Phys. Status Solidi B **245**, 9 (2008).
[13] H. A. Haus, *Waves and Fields in Optoelectronics* (Prentice Hall, Englewood Cliffs, NJ, 1983).